On-chip cell lysis by local hydroxide generation

Dino Di Carlo,† Cristian Ionescu-Zanetti,† Yolanda Zhang, Paul Hung and Luke P. Lee*

Received 26th August 2004, Accepted 9th November 2004
First published as an Advance Article on the web 9th December 2004
DOI: 10.1039/b413139h

We present a novel method for on-chip cell lysis based on local hydroxide electro-generation. Hydroxide ions porate the cell membrane, leading to cell lysis. After lysis occurs, hydrogen ions, also generated on chip, react with excess hydroxide, creating a neutral pH lysate and eliminating the need for a wash step. Three different cell types are shown to be effectively lysed by this method: red blood cells, HeLa (human tumor line) and Chinese Hamster Ovary (CHO) cell lines. The release of cytoplasmic molecules from HeLa and CHO cells is demonstrated by monitoring the escape of a membrane impermeant dye from the cytoplasm. In the vicinity of the cathode, the hydroxide concentration is predicted by finite element simulations and shown to fit the lysis rates at different distances from the generating cathode. For flow-through experiments, a second device integrating a mechanical filter with hydroxide generation is fabricated and tested. The purpose of the filter is to trap whole cells and only allow lysate to pass through. The flow rate dependence of hydroxide concentration at the lysis filter is modeled and lysis efficiency is experimentally determined to be proportional to the hydroxide concentration for flow rates from 15 to 30 μl min^{-1}.

Introduction

Miniaturization of chemical and biological analysis systems has recently gained much attention,[1–4] in the hope that trends similar to those seen in the integrated circuit industry will be applied to microfludic devices. Miniaturization of electronic components on an integrated chip enabled varied and complex applications to be implemented at high speed and low cost. Likewise, development of miniaturized components for chemical and biological assays is important for the implementation of complex analysis tools at low unit cost.[5,6]

In traditional bioanalytical methods the most time consuming and expensive steps involve sample preparation for subsequent detection and analysis, rather then detection itself. Accordingly, emphasis has been placed on developing microfluidic components for sample preparation.[7–11] In preparing biological samples it is often necessary to access intracellular biomolecules. Depending on assay requirements, different methods of on-chip cell lysis have been reported: For protein extraction, detergents such as sodium dodecyl sulfate (SDS) and Triton X-100 have been used successfully for lysis. However, this method necessitates complex devices including injection channels and mixing to homogenize samples.[12–14] In addition, detergents will often interfere with downstream assays and sometimes are not strong enough to effect lysis (as in the case of spores). For DNA analysis, thermal methods are often used since heaters are already necessary for PCR.[8,15] Thermal methods are advantageous as detergents have been shown to interfere with quantitative PCR.[16] Lysis caused by irreversible electroporation has also been reported[17–21] and successfully shown at the single cell level.[17,19] This technique is especially useful if electrodes are already present within the device, as for dielectrophoretic sample processing[18] or electrophoretic separation post-lysis.[19] The disadvantage of this technique is the high field strengths required for lysis (0.3–2 kV cm^{-1}),[17–19] which typically necessitate a high voltage power supply and lead to joule heating of the working fluid[19] and bubble generation.

The method presented here does not require fluid ports or valves for reagent delivery and operates at a low applied voltage of 2.5 V (40 V cm^{-1}), generating the lytic agent locally from the cell-suspending buffer. While microelectrodes have been used previously to control pH for protein separation,[22] our approach is novel in that it uses hydroxide as a reagent for membrane disruption. Unlike lysis by the addition of excess detergent, which remains in the lysate, in our device OH^-, the lytic agent, is quenched downstream by recombination with H^+ ions generated at the anode. While protein unfolding often occurs at elevated pH, a number of proteins have been shown to refold to their native conformation when returned to normal pH.[23,24] Therefore, after a brief exposure to high pH values, many proteins will return to their native conformation. Alkaline conditions induced by sodium hydroxide have been used extensively off-chip in the recovery of plasmid DNA (pH 12.0–12.5)[25] and intracellular recombinant products (pH 10–12.5)[26,27] from large bacterial cultures. Therefore, we present a lysis method based on very simple fabrication and operation that is suitable for both protein and DNA recovery.

Materials and methods

Device design

To demonstrate the ability to effectively lyse cells with locally generated hydroxide, two microfluidic devices containing integrated palladium electrodes were designed. Palladium

† These authors contributed equally.
*lplee@socrates.berkeley.edu

This journal is © The Royal Society of Chemistry 2005

was chosen as the electrode material because it hydrolyses water at low voltages,[28] and is easily patterned by evaporation due to its low melting point (as compared to platinum). The first device contained a single flow chamber with two integrated electrodes (Fig. 1a). The distance between electrodes was 600 μm, resulting in a field strength of 43 V cm^{-1}. The chamber width and length were 1.5 mm × 5 mm. The second device design consisted of ten lysis chambers linked in parallel with equal fluidic resistance for each path (Fig. 2a–b). A filter to keep intact cells until lysis and two electrodes were present in each lysis chamber (Fig. 2c). The chambers had a height of 40 μm and width of 3 mm, while the filter consisted of 145 arrayed channels of only 2 μm in height and width. The parallel design was used because preliminary flow-through experiments on the one-chamber device were hindered by either cell settling within tubing connections to the device at low flow rates or inadequate accumulation of OH^- at higher flow rates. A parallel design allowed higher flow rates within the outside tubing while maintaining a lower flow rate within each lysis chamber.

The palladium electrodes were used to electrochemically generate OH^- and H^+ in the dominant hydrogen and oxygen evolution reactions that occur in aqueous solutions at the cathode and anode:[28]

$$\text{cathode: } 4H_2O + 4e^- \leftrightarrow 4OH^- + 2H_2$$

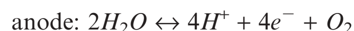

$$\text{anode: } 2H_2O \leftrightarrow 4H^+ + 4e^- + O_2$$

Wear of the generating electrodes was not observed within the time period of the experiments. The devices were re-used for several experiments totaling up to 15 hours with currents of 15 μA per electrode pair without any apparent disintegration of the electrodes. A white residue was observed to form on the anode after about an hour of continuous use, but could be removed by reversing the voltage bias in subsequent experiments.

The use of PDMS for microchannel fabrication had the added benefit of being gas permeable, allowing for complete filling of the device and release of any generated gases.

Another PDMS device, originally designed for on-chip patch clamp measurements,[29] was used for cell trapping and determination of the OH^- concentration necessary to cause fast lysis events. Briefly, this consisted of a microchannel of small cross-sectional area (3 μm × 3 μm) branching out from a larger chamber (200 μm × 50 μm), and was fabricated by PDMS micromolding. A single cell was immobilized at the channel junction by applying negative pressure (−2 psi) to the microchannel (Fig. 3a). Isotonic sodium hydroxide solutions were introduced from the top of the central chamber, resulting in lysis of the trapped cell.

Microfabrication

Fabrication of the electrochemical devices proceeded as follows: electrodes were photolithographically defined onto a

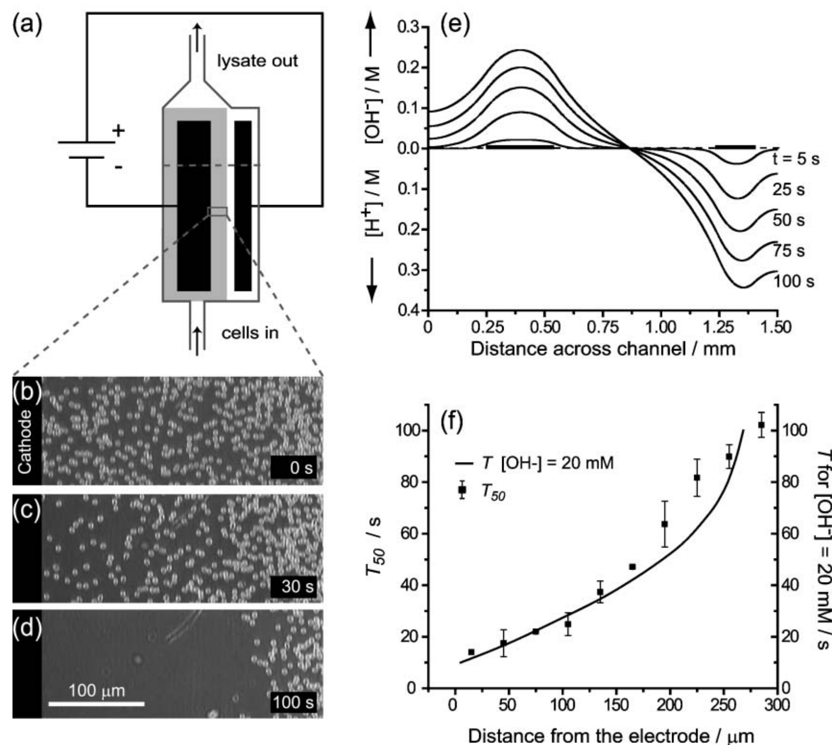

Fig. 1 Spatio-temporal distribution of lysis events in hydroxide gradients. (a) A schematic of a microfabricated device for local hydroxide production by the electrolysis of water at the cathode is shown. The cell suspension is introduced into the lysis chamber from the bottom and the lysis area is indicated in grey. (b–d) Movie frames showing changes in the red blood cell density due to lysis inside the device. Lysis proceeds in a similar fashion around all sides of the cathode (grey region, a). Here, the edge of the cathode is at the left of the image. (e) Simulation results for the OH^- and H^+ concentration along a cross section through the device (dashed line in (a)). (f) The time scale for 50% cell lysis as a function of distance from the electrode is plotted along with the time required for hydroxide ions to diffuse in and reach the lytic concentration ($[OH^-]$ = 20 mM). The error bars represent standard deviation of data from three movies.

This journal is © The Royal Society of Chemistry 2005

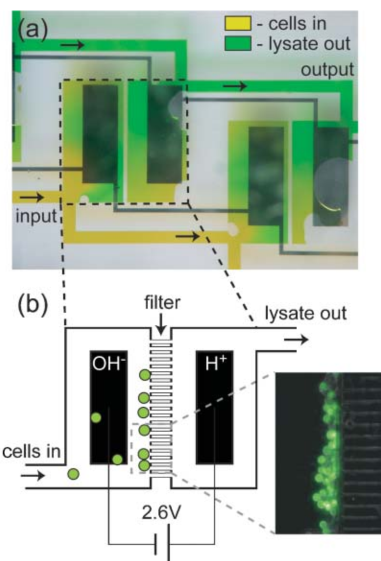

Fig. 2 A filter device for flow-through hydroxide lysis. (a) Two parallel lysis chambers are shown from a 10-chamber device. Yellow dye indicates regions where cells are flowed in (from left to right), while green dye regions show where the lysate flows out. Palladium electrodes are separated by a filter region of lower channel height. (b) Schematic of lysis chamber operation. To produce hydroxide for lysis 2.6 V is applied across the electrodes. Hydroxide is formed at the cathode (upstream) while H^+ forms at the anode on the other side of the filter (downstream). Cells are trapped at the filter until lysis. Recombination of excess OH^- and H^+ downstream leads to a neutral lysate. An inset of the filter region shows trapped calcein stained HeLa cells overlaid on a bright field image of the filter.

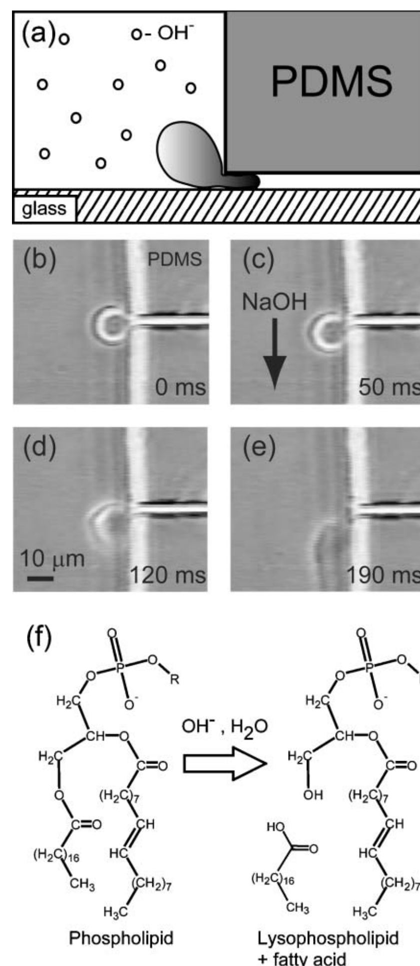

Fig. 3 Sodium hydroxide lysis of trapped cells. (a–e) Frames from a movie of alkaline lysis for a single cell trapped in a microfluidic device. The cell is trapped by applying suction to a small channel on the side of a larger chamber. An isotonic alkaline solution (50 mM NaOH in PBS) is introduced into the main chamber from the top (arrow, c). Colloid-osmotic lysis happens over a time scale of 190 ms. (f) The reaction responsible for cleaving the fatty acid groups of membrane phospholipids, leading to the creation of lysophospholipids which have been shown to induce membrane permeabilization.

glass slide. Titanium (Ti, 10 nm) and palladium (Pd, 150 nm) were then e-beam evaporated followed by photoresist lift-off in acetone. Titanium was used as an adhesion layer. The molds for the microfluidic channels and lysing chambers were fabricated using negative photoresist (SU-8 25, Microchem Corporation, 40 μm thick). Poly-dimethylsiloxane (PDMS, Sylgard 184, Dow Corning) was poured on the mold and cured in a 70 °C oven for 6 hours. The PDMS was then carefully peeled off the mold. The fluid inlet and outlet were punched by a flat-tip needle for tube connections. Both the glass slide with Ti/Pd electrodes and the PDMS structures were treated with oxygen plasma (2 Torr, 40 W) for 40 seconds before bonding. The PDMS was then carefully aligned and bonded to the glass slide so that the chamber entirely covered the electrodes on the glass slide.

Single cell lysis events

Three different cell lines were used. Red blood cell experiments were performed with defibrinated sheep's blood (HemoStat Labs, Dixon, CA) diluted 20 times in phosphate buffered saline (PBS). The other cell lines tested were HeLa cells (a human tumor cell line) and CHO (chinese hamster ovary) cells, which are commonly used cell culture lines. Adherent cell lines were grown in DMEM + 10% FBS (Gibco) and passaged twice weekly. To determine membrane rupture and release of cytoplasmic molecules in the HeLa and CHO cell lines, dye loading was performed by adding calcein AM (Molecular Probes, 10 μg ml^{-1}, M = 1 kD) to the cell suspension and incubating the cells for 20 min. After centrifugation and replacement with fresh PBS, HeLa cells were introduced into the lysis chamber. Flow was stopped by closing external valves and fluorescent time-lapse microscopy was performed while OH^- was being diffused into the extracellular solution using the single-chamber device. For RBC experiments, 2.5% hematocrit solutions were introduced into the single-chamber device with stopped flow. Current was set to 15 μA and lysis as a function of distance and time was measured by optical microscopy. All fluorescence and brightfield images were taken with a Nikon inverted microscope using either a mercury arc or incandescent lamp as a light source. Images were collected with a Cascade 512B digital camera (Roper Scientific, Tucson, AZ) with the CCD cooled to −20 °C. Further image processing and dye intensity analysis was performed using MATLAB (The MathWorks, Natick, MA). For HeLa and

CHO cells, calcein flux out of the cell is measured by integrating dye intensity over the cell area.

Flow-through cell lysis measurements

For flow rate dependent cell lysis measurements, HeLa cells in PBS solution were loaded with calcein AM. A stock solution of calcein AM (1 mM in DMSO) was added to the cell suspension (4 μM) and incubated at 37 °C for 20 min. For the experiments presented calcein AM containing solution was not replaced after cell loading. The cell concentration for flow-through experiments was $\sim 1.5 \times 10^6$ cells ml^{-1}. Prior to introducing cells the device was loaded with PBS and pressurized using a syringe with a closed outlet to remove any air trapped inside. After engaging a new syringe with cell solution in a syringe pump the PBS filled syringe was carefully replaced. Flow was initiated until a background level of fluorescence was observed from the cell solution. Next, −2.6 V was applied to the cathode and fluorescence intensity of the bulk solution was recorded over time at the common outlet of all 10 lysis chambers. Typical currents of 120–180 μA were recorded for 10 parallel lysis chambers. The device was washed with PBS after each flow rate experiment to remove any remaining debris and fluorescent molecules. To control for fluorescent intensity changes due to hydrolysis of calcein AM esters by the hydroxide generated on chip, separate experiments were performed with 4 μM calcein AM solution in PBS (excluding cells).

Simulations

To estimate OH^- concentration profiles within the lysis chambers at various flow rates, multiphysics simulations of coupled fluid flow and mass transport were conducted using FEMLAB software (Comsol Inc., Burlington, MA). For the parallel (second) device design the following assumptions were made. Considering the symmetry of the device, computational time was decreased by simulating a single lysis chamber. Also, since each lysis chamber has a large aspect ratio (3 mm wide, 3 mm long, and 40 μm in height), a 2D approximation of the domain was appropriate. Because the lysis filter channels are only 2 μm high the actual fluidic resistance in these channels was modeled in the 2D simulation by increasing the channel length and decreasing the number of channels. For the first, single-chamber, device a 2D approximation was also applied to the domain (1.5 mm × 5 mm × 40 μm). The experiments in this device were conducted on stationary cells in suspension so diffusive flux was simulated in the absence of fluid flow.

However, for a steady state solution in the parallel device the two problems were decoupled to ease computation. First, the fluid dynamics problem was solved using the incompressible Navier–Stokes equations. The fluid velocity at the inlet was specified based on a channel width of 300 μm, height of 40 μm, and a given flow rate. For a flow rate of 10 $\mu L\ min^{-1}$ through 10 parallel devices an inlet velocity of 1.39 mm s^{-1} was calculated. The outlet was given a constant pressure boundary condition. The viscosity used for the cell suspension was 1 mPa s.

Once the fluid flow problem was solved for the parallel device, steady-state mass transport was found using a convection-diffusion equation with sources and sinks. Since the concentrations of OH^- produced are orders of magnitude less than the supporting electrolyte (PBS ~ 150 mM), contributions from electro-migration to mass transport are negligible compared to convection and diffusion.[30] For a constant diffusion coefficient of OH^- in buffered solutions ($D = 5 \times 10^{-6}$ $cm^2\ sec^{-1}$),[31,32] the equation becomes:

$$-D\nabla^2 C = R - \vec{u} \cdot \nabla C \quad (1)$$

where C is the concentration of OH^- and u is the fluid velocity vector. The source, R, was determined from the average current per device (i =15 μA) at a bias of 2.6 V.[30]

$$R = i/nFV \quad (2)$$

Assuming an equal generation of OH^- over the surface of the cathode, with a width of 0.85 mm and length of 2.4 mm then V = 81.6 pL. The number of electrons (n) used per OH^- ion is 1 and F is Faraday's constant. H^+ ions were also generated at the anode with the same parameters. When H^+ and OH^- ions occupied the same spatial coordinates they were assumed to combine to form water with the equilibrium constant $K = 10^{-14}$.

For the single-chamber device similar analysis was performed to determine the time-dependent concentration distribution without fluid flow. Here an applied current of 15 μA was used over the cathode area (3 mm × 300 μm) and anode area (3 mm × 150 μm).

For the convective–diffusive equations, the inlet boundary condition was that of a constant OH^- concentration (10^{-7} M) corresponding to a pH 7 buffer. The outlet condition was that of zero concentration gradient across the boundary.

Results and discussion

[OH^-] required for cell lysis

Trapped cells were exposed to NaOH solutions of various hydroxide concentrations in order to determine the amount of OH^- necessary for fast lysis. HeLa cells were first trapped in a microfluidic device developed previously for patch clamp recording as shown in Fig. 3a (see Materials and Methods).[29] Cell lysis (Fig. 3b–e) occurs after an isotonic solution of 50 mM hydroxide (NaOH) in PBS (pH 12.28) was flowed into the device. In an alkali environment, excess hydroxide is known to cleave the fatty acid–glycerol ester bonds in phospholipid molecules, resulting in the production of fatty acid chains and lysophospholipids (Fig. 3f).[33,34] Single cells were lysed quickly by isotonic solutions of 100 mM OH^- in PBS (pH 12.55) down to 20 mM OH^- in PBS (pH 11.70), but not for 10 mM OH^- in PBS (pH 11.20). From these experiments we found 20 mM to be a characteristic hydroxide concentration required for fast cell lysis.

Spatio-temporal distribution of lysis events

In an RBC filled device, time-dependent cell lysis was observed in the vicinity of the cathode (grey region Fig. 1a). In the vicinity of the anode, where acidic conditions prevail, lysis did

This journal is © The Royal Society of Chemistry 2005

not occur within the observed time (t = 3 min). This is in agreement with Jin *et al.*,[35] since low pH 1–2 is generated at the anode over this time period. For a PBS filled device, a large increase in current and hydrogen (H_2) bubble nucleation are observed at applied voltages above 2.5 V across the electrodes (data not shown). Therefore, we conducted our experiments at a bias of 2.6 V, where hydrolysis dominates charge transfer at the electrodes, but bubble nucleation was only observed under no flow conditions and after long periods of time ($t > 2$ min).

It is instructive to look at the temporal and spatial distribution of lysis events. We observe lysis to proceed from the cathode edge outwards in all directions (grey region, Fig. 1a). This confirms that lysis is not due to the electric field between the electrodes because lysis proceeds similarly in areas of zero electric field (left half of grey region, Fig. 1a). Additionally, the electric field was only 43 V cm^{-1}, an order of magnitude below those reported for electroporation based lysis, which varied from 0.3–2 kV cm^{-1}.[17–19]

The number of lysis events as a function of time and distance from the electrode was calculated by measuring the cell density from images such as those shown in Fig. 1b–d. Lysis proceeds from the left side of the picture, starting at the edge of the cathode. The time required for 50% lysis of the initial cell population (T_{50}) for different vertical strips of the image is plotted as a function of the distance from the cathode (Fig. 1f, black squares). Because the height of the chamber is small compared to its width (40 μm *vs.* 1.5 mm), we assume a constant hydroxide concentration for each vertical slice at a distance x from the electrode edge. Simulating the OH^- and H^+ generation and diffusion yields a time-dependent concentration distribution (Fig. 1e). Since we have determined lysis to occur when $[OH^-]$ = 20 mM, the time needed to reach that concentration at a distance x from the electrode can be found from our simulation. The simulation results, based on a reported hydroxide diffusion constant of $D_{OH} = 4.6 \times 10^{-6}$ cm^2 s^{-1},[31,32] agrees well (standard deviation = 8.32 s) with the measured time to 50% lysis (black squares, Fig. 1f). This confirms the fact that hydroxide is the lytic agent. While lysis of the entire cell population occurs over 2 minutes, it is made up of individual cell lysis events that are scattered in time but occur on very short time scales ($\Delta t < 100$ ms for RBCs).

Release of cytoplasmic contents during single cell lysis

For individual cells in a single-chamber device, the voltage applied to the electrodes (2.6 V) results in a steady increase of the local hydroxide concentration. Hydroxide is known to cleave membrane phospholipids into fatty acids and lysophospholipids.[33,34,36] In turn, lysophospholipids have been previously shown to lead to lysis by the colloid-osmotic mechanism when added to extracellular solution,[37–39] which strongly suggests lysophospholipid driven membrane poration as the cause of alkaline lysis.

Because RBCs do not contain intracellular esterases that allow internalization of fluorescently-active calcein, only phase contrast data were collected. Several seconds prior to the fast radial change and lysis event a transition to a spheroid morphology is observed for the RBCs, consistent with previous reports.[40] During the fast lysis event, the RBC radius expands by an average of 42 ± 10%, with a characteristic time scale for the radial change of 60 ms (data not shown).

HeLa and CHO cells were convenient model systems because of their large size and our ability to use the cytoplasmic dye calcein AM for fluorescence measurements (see Materials and Methods). A representative HeLa cell lysis event is shown in Fig. 4. We found the fast lysis event to last 159 ± 64 ms for HeLa cells (n = 20). Cell radius was calculated by averaging the width at half maximum for three cross-sectional intensity plots. The radial change for the cell in Fig. 4a–c is plotted as a function of time in Fig. 4d (solid red circles) and fitted by a boltzmann sigmoidal function (dashed red line, $\chi^2 = 3.7 \times 10^{-5}$). Radial expansion is driven by lysophospholipid mediated pore formation. This leads to mobile ion flux and an osmotic imbalance due to the fixed charge on membrane impermeant intracellular proteins. During this imbalance water molecules entering the cytoplasm induce an intracellular pressure that causes membrane expansion and further increases in pore radius. When the pores expand beyond a given size, the dye molecules (calcein, diameter ≈ 1.6 nm) exit the cell. The total amount of dye in the cytoplasm was obtained by integrating the fluorescent intensity of the cell shown in Fig. 4a–c. This is plotted together with the radial change in Fig. 4d (open blue circles), and is fit well by a sigmoidal function (solid blue line, $\chi^2 = 3.0 \times 10^{-5}$). The data indicate the presence of a critical level of membrane permeation, after which fast radial expansion ensues.

For CHO cells, a similar analysis of single cell lysis events was performed. In contrast with HeLa cells, the lysis event occurs over a longer time of 2.11 ± 0.54 s (n = 8). Additionally, an initial phase of dye loss preceded radial change in these cells (Fig. 5d). A radial change for the cell in Fig. 5a–c is plotted as a function of time in Fig. 5d (solid red

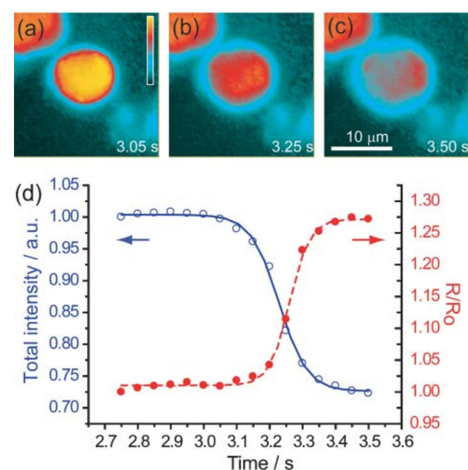

Fig. 4 Membrane permeabilization and lysis of HeLa cells. (a–c) Pseudocolor fluorescent images contain information on both the radial expansion and the escape of cytoplasmic dye during lysis. A HeLa cell loaded with a cytoplasmic dye (calcein AM) is being lysed by the application of hydroxide to the membrane (generating electrode to the far left). (d) Radial expansion of the cell (dashed red line, right y-axis) and the total cytoplasmic dye loss (solid blue line, left y-axis) during the lysis event are plotted as a function of time and fitted by sigmoidal functions.

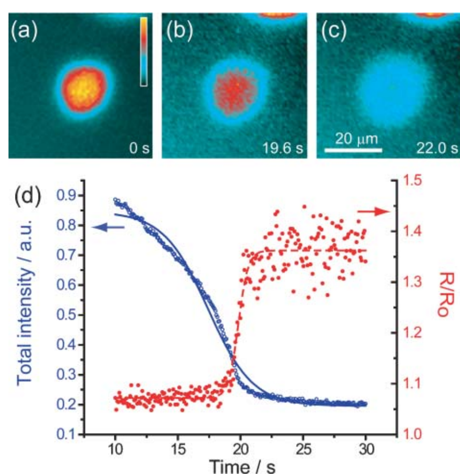

Fig. 5 Membrane permeabilization and lysis of CHO cells. (a–c) Pseudocolor fluorescent images contain information on both the radial expansion and the escape of cytoplasmic dye during lysis. A CHO cell loaded with a cytoplasmic dye (calcein AM) is being lysed by the application of hydroxide to the membrane (generating electrode to the far left). (d) Radial expansion of the cell (dashed red line, right *y*-axis) and the total cytoplasmic dye loss (solid blue line, left *y*-axis) during the lysis event are plotted as a function of time and fitted by sigmoidal functions. An average time scale of 2.11 ± 0.54 seconds was observed for the transition in cell radius (data from 8 cells).

circles) and fitted as before (dashed red line, $\chi^2 = 8.5 \times 10^{-4}$). Fluorescence intensity is plotted together with the radial change in Fig. 5d (open blue circles), and is also fit by a sigmoidal function (solid blue line, $\chi^2 = 4.9 \times 10^{-4}$). Differing cell size and membrane properties between cell types may account for variation in dye leak and fast lysis time scales.

Simulation results

For the parallel device (Fig. 2), the geometry of the lysis chamber was modeled in 2D as described in the experimental section. Both OH^- and H^+ steady state concentration distributions were modeled for flow rates from 10–90 μl min^{-1}. The concentration distribution for a flow rate of 10 μl min^{-1} is plotted in Fig. 6a. Because asymmetry in the flow leads to asymmetry in convection of electrogenerated products, the distribution of OH^- near the chamber filter is not uniform. Cells at the filter (Fig. 6a, dashed line) are exposed to a small pH gradient. An average pH at the filter is obtained from the average OH^- concentration and is plotted as a function of flow rate (Fig. 6c, dotted line). A Peclet number, $P = UL/D$, can be defined as the ratio of convective to diffusive mass transport. For flow rates of 10–90 μl min^{-1} P varied from 5.7–51 at the filter, indicating a convection dominated solution. As convective contributions to mass transport increase (*i.e.* faster flow rates) the OH^- level at the filter decreases.

Previously we have determined that fast lysis occurs for HeLa cells above pH 11.70. Macrophages have been shown to lyse at pH 13 in less than 60 seconds while taking more than 120 seconds at pH 12.[35] Combining these results with the modeling data shown in Fig. 6 suggests a range of flow rates at which lysis should occur (0–20 μl min^{-1}). At the outlet of the lysis chamber recombination of H^+ and OH^- will return proteins and other biomolecules to neutral pH. To enhance this process, after exiting the outlet of one lysis chamber the stream of lysate is laminated with the streams exiting the neighboring lysis chambers in an alternating fashion (high pH, low pH, high pH, …). This arrangement reduces the diffusion path and mixing time to reach a neutral lysate.

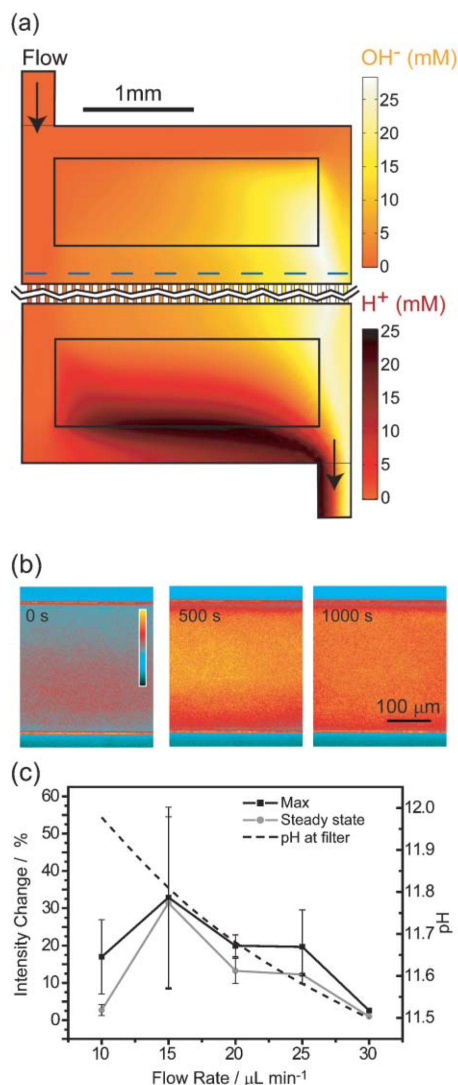

Fig. 6 Lysis data compared to simulation results. (a) Simulation of the concentration distribution of OH^- and H^+ in one lysis chamber for a flow rate of 1 μl min^{-1} per chamber. Flow comes in from the top left and exits from the bottom right. Electrodes are shown as rectangles in the centers of the chamber separated by a filter. Results in the filter region, which was elongated to match fluidic resistance, are not shown. (b) Pseudocolor images from one device that were used to calculate the average fluorescence intensity at the common outlet. Images are shown at various times for a flow rate of 20 μl min^{-1}. (c) Intensity change is plotted as a function of flow rate indicating both the maximum intensity increase and intensity after reaching a steady state value 1000 s after voltage application. Simulated pH as a function of flow rate is plotted against the right axis for comparison.

This journal is © The Royal Society of Chemistry 2005

Flow-through cell lysis measurements

Using the flow rates suggested by finite element modeling as a guide, experiments were conducted to determine the flow rate for which maximal cell lysis occurs. HeLa cells were loaded with the cytoplamic dye calcein AM and injected into the devices (see Materials and Methods). If the calcein AM solution was replaced by PBS no signal above baseline was observed. At a lysis rate of 50 cells min^{-1} at each filter and a low flow rate of 15 μL min^{-1} the dye intensity due to calcein release from the cell is calculated to be six orders of magnitude below the cell intensity, therefore not detectable at the outlet. We therefore designed a different experiment: cells are kept in the buffer containing calcein AM during lysis, such that the release of intracellular esterases after lysis resulted in accelerated conversion of extracellular calcein AM to calcein, and a detectable fluorescent signal at the outlet (Fig. 6b). An additional advantage of this setup is the ability to verify the functionality of esterases after exiting the cytoplasm. Hydrolysis of calcein AM esters by hydroxide was shown to be irrelevant by running a control where buffer containing calcein AM is flowed through the device in the absence of cells at the same bias voltage. Less than a 1% increase in fluorescence was observed at the outlet in this case (data not shown).

For cell experiments, no intensity change is detected in the absence of an electrode bias. When a 15 μA current is passed between the electrdoes per chamber, the fluorescence at the device outlet varies as a function of flow rate. We plot data averaged from two devices for both maximum and steady state intensity at the outlet (Fig. 6c). There is a trend of increased intensity as the flow rate decreases that corresponds well with the increased average pH at the filter (Fig. 6c, dotted line). The exception is the 10 μl min^{-1} data point, where the steady state intensity decreases due to either cell settling in the outside tubing or irreversible denaturation of intracellular esterases. The fact that increased fluorescence intensity upon lysis is only observed when calcein AM remains in solution and there is no observed calcein AM hydrolysis, shows that cytosolic proteins (esterases) are released and function even after exposure to elevated pH. In the future, flow-through lysis may be enhanced by replacing the PDMS filter with a nanostructured Si filter that has been shown to lead to mechanical cell lysis.[41]

Recently, there has been interest in the on-chip disruption of bacterial spore coats. Because of the many protective protein layers, intracellular biomolecules can often not be accessed using thermal or chemical treatments alone.[42] Exposure to 0.1 M NaOH has been shown to aid in the solubilization of spore coat proteins in *Bacillus subtilis*.[42] Mechanical methods like sonication with glass beads have also been successfully miniaturized to access intra-spore DNA.[43] Therefore, concurrent treatment with locally generated OH^- may be a complementary technique to reduce time or sonication energy in bead-based lysis.

Conclusions

We have demonstrated cell lysis by on-chip electrogeneration of the lytic agent (hydroxide). Hydroxide is confirmed as the lytic agent by several pieces of evidence: (i) Lysis was not observed at the anode where H^+ is generated. (ii) Lysis occurs even in regions of no electric field. (iii) Hydroxide solution was shown to lyse cells at 20 mM [OH^-], which is present at the cathode during lysis according to simulation results. (iv) The distribution in lysis times as a function of distance agrees with the diffusion constant of OH^- in buffered solutions. (v) Flow-through data shows an increased lysis efficiency that corresponds with increased hydroxide concentration.

Three cell types (RBCs, HeLa, and CHO) have been shown to lyse by this method. For HeLa and CHO cells, release of cytoplasmic contents was quantified by measuring leak of the membrane impermeant dye calcein (1 kD) during the lysis event. This data was collected from single cell lysis experiments under zero flow conditions. For flow-through experiments, the release of functioning esterases from HeLa cells was measured and compared to the pH at the lysis filter.

The principle advantages of this lysis method are: (i) no need for a wash/dialysis step after lysis, (ii) reduced device design complexity, without pumps and input ports, (iii) low working voltage (2.6 V) and power consumption (30 μW), and (iv) real time control of lytic agent generation.

Acknowledgements

This work is partially supported by a Whitaker Foundation Graduate Fellowship (D. D.).

Dino Di Carlo,† Cristian Ionescu-Zanetti,† Yolanda Zhang, Paul Hung and Luke P. Lee*
Department of Bioengineering, University of California at Berkeley, Berkeley, CA, USA. E-mail: lplee@socrates.berkeley.edu; Fax: +1 510-642-5880; Tel: +1 510-642-5855

References

1 B. H. Weigl and P. Yager, *Science*, 1999, **283**, 346–347.
2 L. R. Huang, E. C. Cox, R. H. Austin and J. C. Sturm, *Science*, 2004, **304**, 987–990.
3 D. J. Beebe, J. S. Moore, J. M. Bauer, Q. Yu, R. H. Liu, C. Devadoss and B. H. Jo, *Nature*, 2000, **404**, 588–590.
4 G. M. Whitesides, *Nat. Biotechnol.*, 2003, **21**, 1161–1165.
5 T. Thorsen, S. J. Maerkl and S. R. Quake, *Science*, 2002, **298**, 580–584.
6 J. Liu, C. Hansen and S. R. Quake, *Anal. Chem.*, 2003, **75**, 4718–4723.
7 Y. Huang, E. L. Mather, J. L. Bell and M. Madou, *Anal. Bioanal. Chem.*, 2002, **372**, 49–65.★ This paper reviews the important aspects of sample preparation with emphasis on cell lysis.
8 R. H. Liu, J. Yang, R. Lenigk, J. Bonanno and P. Grodzinski, *Anal. Chem.*, 2004, **76**, 1824–1831.
9 A. Hatch, E. Garcia and P. Yager, *Proc. IEEE*, 2004, **92**, 126–139.
10 J. Lichtenberg, N. F. de Rooij and E. Verpoorte, *Talanta*, 2002, **56**, 233–266.
11 A. J. de Mello and N. Beard, *Lab Chip*, 2003, **3**, 11N–19N.★ A review of sample preparation in microfluidics for real samples.
12 P. C. H. Li and D. J. Harrison, *Anal. Chem.*, 1997, **69**, 1564–1568.
13 G. Ocvirk, H. Salimi-Moosavi, R. J. Szarka, E. A. Arriaga, P. E. Andersson, R. Smith, N. J. Dovichi and D. J. Harrison, *Proc. IEEE*, 2004, **92**, 115–125.
14 E. A. Schilling, A. E. Kamholz and P. Yager, *Anal. Chem.*, 2002, **74**, 1798–1804.
15 L. C. Waters, S. C. Jacobson, N. Kroutchinina, J. Khandurina, R. S. Foote and J. M. Ramsey, *Anal. Chem.*, 1998, **70**, 158–162.
16 A. Abolmaaty, M. G. El-Shemy, M. F. Khallaf and R. E. Levin, *J. Microbiol. Methods*, 1998, **34**, 133–141.
17 J. Gao, X. F. Yin and Z. L. Fang, *Lab Chip*, 2004, **4**, 47–52.

This journal is © The Royal Society of Chemistry 2005

18 P. R. C. Gascoyne and J. V. Vykoukal, *Proc. IEEE*, 2004, **92**, 22–42.
19 M. A. McClain, C. T. Culbertson, S. C. Jacobson, N. L. Allbritton, C. E. Sims and J. M. Ramsey, *Anal. Chem.*, 2003, **75**, 5646–5655.
20 S. W. Lee and Y. C. Tai, *Sens. Actuators, A: Phys.*, 1999, **73**, 74–79.
21 J. Cheng, E. L. Sheldon, L. Wu, M. J. Heller and J. P. O'Connell, *Anal. Chem.*, 1998, **70**, 2321–2326.
22 K. Macounova, C. Cabrera, M. Holl and P. Yager, *Anal. Chem.*, 2000, **72**, 3745–3751.★ This paper shows the generation of pH gradients on chip using electrolysis of water.
23 E. Jaspard, *Arch. Biochem. Biophys.*, 2000, **375**, 220–228.
24 H. Kristinsson and H. Hultin, *J. Agric. Food Chem.*, 2004, **52**, 3633–3643.
25 H. C. Birnboim and J. Doly, *Nucleic Acids Res.*, 1979, **7**, 1513–1523.
26 S. T. L. Harrison, J. S. Dennis and H. A. Chase, *Bioseparation*, 1991, **2**, 95–105.
27 S. T. L. Harrison, *Biotechnol. Adv.*, 1991, **9**, 217–240.
28 C. Sanchez, E. Leiva and W. Schmickler, *Electrochem. Commun.*, 2003, **5**, 584–586.
29 J. Seo, C. Ionescu-Zanetti, J. Diamond, R. Lal and L. Lee, *Appl. Phys. Lett.*, 2004, **84**, 1973–1975.
30 A. J. Bard and L. R. Faulkner, *Electrochemical Methods*, John Wiley & Sons: New York, 2001, pp 307–310.
31 N. Agmon, *Chem. Phys. Lett.*, 2000, **319**, 247–252.
32 N. F. Albaldawi and R. F. Abercrombie, *Biophys. J.*, 1992, **61**, 1470–1479.
33 J. Arnhold, A. Osipov, H. Spalteholz, O. Panasenko and J. Schiller, *Biochim. Biophys. Acta: Gen. Subjects*, 2002, **1572**, 91–100.
34 K. Woo and J. Kim, *J. Chromatogr., A*, 1999, **862**, 199–208.
35 W. R. Jin, Q. Dong, X. Y. Ye and D. Q. Yu, *Anal. Biochem.*, 2000, **285**, 255–259.
36 O. Valiente, L. Mauri, R. Casellato, L. Fernandez and S. Sonnino, *J. Lipid Res.*, 2001, **42**, 1318–1324.
37 T. J. Bierbaum, S. R. Bouma and W. H. Huestis, *Biochim. Biophys. Acta*, 1979, **555**, 102–110.
38 Y. Song and R. Ochi, *Biophys. J.*, 2002, **82**, 96A–97A.
39 H. U. Weltzien, *Biochim. Biophys. Acta*, 1979, **559**, 259–287.
40 R. W. Harris, P. J. Sims and R. K. Tweten, *Infect. Immun.*, 1991, **59**, 2499–2501.
41 D. Di Carlo, K. H. Jeong and L. P. Lee, *Lab Chip*, 2003, **3**, 287–291.
42 H. Takamatsu and K. Watabe, *Cell. Mol. Life Sci.*, 2002, **59**, 434–444.
43 P. Belgrader, D. Hansford, G. T. A. Kovacs, K. Venkateswaran, R. Mariella, F. Milanovich, S. Nasarabadi, M. Okuzumi, F. Pourahmadi and M. A. Northrup, *Anal. Chem.*, 1999, **71**, 4232–4236.

This journal is © The Royal Society of Chemistry 2005